Weigh-In-Motion System Using a MEMS Accelerometer

Ravneet Bajwa
Pravin Varaiya

Electrical Engineering and Computer Sciences
University of California at Berkeley

Technical Report No. UCB/EECS-2009-127
http://www.eecs.berkeley.edu/Pubs/TechRpts/2009/EECS-2009-127.html

September 1, 2009

Abstract

Weigh-In-Motion System Using a MEMS Accelerometer

by

Ravneet S. Bajwa

Master of Science in Electrical Engineering and Computer Science

University of California, Berkeley

Professor Pravin Varaiya, Chair

Weigh stations are separate areas along the highways where trucks are stopped and weighed. Weigh-In-Motion (WIM) systems offer a convenient replacement for weigh stations as they can estimate the load of a moving truck without disrupting the traffic flow. However, current technologies in WIM systems are either very costly or lack accuracy. In this report, a low cost Weigh-In-Motion system using a MEMS accelerometer is proposed. The system uses transient vibrations of the pavement to estimate dynamic load of the moving truck.

A fully functional sensor board, capable of measuring the low amplitude transient vibrations of the pavement due to a dynamic load, was developed and tested. A model for sensor output is proposed and the device is thoroughly calibrated to determine the various parameters included in the model. The sensor can successfully resolve accelerations less than 200 μg and compared well with a reference accelerometer when tested for its frequency response.

The sensor was installed in a concrete pavement and it was tested to be immune to sound and other external noise on the road. A Falling Weight Deflectometer (FWD), which simulates the load applied by an actual truck, was used to excite the pavement and the data collected from our sensor compared well with data collected from FWD's sensors. A low weight truck, although much lighter than commercial trucks, was driven over the sensor and the sensor successfully measured the resulting vibrations in the pavement. In addition, the measured signal was used to identify the individual axles.

Author's Note: This report, along with more future work, will be used as author's M.S. thesis and the purpose of this report is to summarize the work done so far.

Contents

List of Figures

List of Tables

Acknowledgments

I would like to thank my advisor Pravin Varaiya for his immense support and guidance during my last two years at Berkeley. Without any doubt, he is the most understanding (coolest!) advisor and the best mentor I have ever had. I would also like to thank my senior group member Ram Rajagopal for his help and support throughout the project, and for giving me helpful technical and career advice. Many thanks to Bharathwaj Muthuswamy (Bart), Carl Chun, and Raffi Sevlian for all the mind stimulating conversations and lab support. A million thanks to Ferenc, Winthrop, Pete, Tho and Ming of the Electronic Support Group for their assistance with electronic equipment throughout the project. Many thanks to Robert Kavaler, from Sensys Networks, for his help with printed circuit board design. I am very grateful to Professor Harvey and his staff, from UC Davis, for providing help with FWD tests. Thanks to Professor Martin Graham for providing insights on building low noise electronic circuits. Last but not the least, I would specially like to thank my family for their continued love and support.

Chapter 1

Introduction

1.1 Introduction to Weigh-In-Motion (WIM)

Weigh-In-Motion is the process of estimating the weight of a moving vehicle and the portion of that weight carried by each axle. This technology replaces the traditional Weigh Stations, where a truck is stopped and weighed. Estimating the dynamic load of a moving truck is of great importance since this provides a more realistic picture of how much damage the truck is causing to the pavement. In addition, it makes possible the weight measurement of a truck without disrupting the traffic flow. This project aims at building a WIM system using a MEMS accelerometer which measures the extremely low amplitude transient vibrations caused by a moving truck on the pavement. The measured accelerations can then be used to estimate the weight of the moving load [12]. There are 3 different sensors currently used in WIM systems but they all have shortcomings. The following comparison helps us understand their advantages and disadvantages [10].

1.1.1 Bending Plate

Bending plate is a metal plate with a strain gauge attached at the bottom. When a vehicle passes over the sensor, the strain is measured and converted into the dynamic load applied by the vehicle. The advantages of this sensor are that it can be used at both high and low speeds, and its accuracy is high, approximately 10 percent. But the sensor is expensive and hard to install and maintain.

1.1.2 Load Cell

Load cells are transducers used for the measurement of force or weight, usually based on a strain gauge bridge or vibrating wire sensor. A load cell WIM system uses a single load cell with two scales to detect an axle and weigh the right and left sides of the axle simultaneously. As a vehicle passes over the load cell, the system records the weights measured by each scale and adds them together to obtain the axle weight [14]. The load cell is the most accurate in commercially available WIM sensors, about 6 percent. But this is also very expensive and cumbersome to install and maintain.

1.1.3 Piezoelectric Sensor

The piezoelectric sensor converts any pressure applied to electric charge. The measured voltage can then be converted into the dynamic load. This sensor is very cheap and easy to use but its accuracy is lower, about 15 percent.

1.1.4 Accelerometer

The accelerometer based WIM system would be very cheap and easy to install but its accuracy has yet to be determined. A WIM system using an accelerometer would convert the transient vibrations of the pavement to the dynamic load by using the model developed in [12].

1.2 Outline of the Report

In chapter 2, we discuss the model of the pavement, the requirements imposed by this model on the sensor, and the sensor selection. Chapter 3 deals with the design of the electronic board using the sensor and the packaging needed to isolate external noise from the useful pavement vibrations. In chapter 4, we explain the detailed calibration procedure followed and summarize the results of this calibration. In chapter 5, we discuss in detail the experiments done after installing the sensor in a concrete pavement. Last but not least, in chapter 6 we explain the work in progress and the future work to be done.

Chapter 2

Sensor Selection and Board Design

In this chapter, we discuss the model developed in [12] that serves as the foundation of our proposed WIM system. Using the model and the simulations from [12], we define the requirements on our sensor board for it to successfully measure the transient vibrations in the pavement. In the rest of the chapter we discuss how the sensor was chosen, the trade-offs involved, and the initial performance of the sensor on a prototype board.

2.1 Model Used for the WIM system

Rajagopal et al. modeled the pavement as a one dimensional Euler beam with elastic foundation, described by the following PDE [12]:

$$EI\frac{\partial^4 y}{\partial x^4} + \gamma\frac{\partial^2 y}{\partial t^2} + \kappa\frac{\partial y}{\partial t} + \beta y = F(x,t). \tag{2.1}$$

Here x is the horizontal position along the road, $y(x,t)$ is the vertical displacement of the pavement, $F(x,t)$ is the non-stationary force acting on the pavement due to the transient dynamic loads applied through the tires of the moving vehicle at position x and time t. This force resulting from a truck, moving at velocity (v) was modeled as:

$$F(x,t) = F(1 + \eta\cos(\omega_0 t)) \times \delta(x - vt). \tag{2.2}$$

Here η can range between 0 and 1, depending on whether the pavement surface is smooth or rough. It was shown in [12] that as L$\rightarrow \infty$ the solution to the PDE is given by:

$$\lim_{L\rightarrow\infty} y(x,t) = F_0 Re[\psi^*(vt - x)e^{j\omega_0 t}] + O(e^{-kt}), \tag{2.3}$$

where

$$\begin{aligned} \psi^*(t) &= \frac{1}{2\pi i}\int_{-\infty}^{\infty} \Omega(s)^{-1} e^{st} ds, \\ \Omega(s) &= \frac{\alpha s^4}{\gamma} + v^2 s^2 + (2\omega_0 vi + 2kv)s + (\frac{\beta}{\gamma} - \omega_0^2 + 2kw_0 i). \end{aligned}$$

Figure 2.1 shows the relative mean square difference (in percent) between the ground truth solution of the PDE, given by equation (2.1), and the asymptotic approximation given by equation (2.3). A fixed position, $x = L/2$, was chosen as we are only interested in the behavior away from the virtual boundaries of the pavement. Also, a load of 10000 N moving at $v = 10$ m/s was used to compute the solutions. It is clear from the figure that the error becomes negligible for lengths greater than 50 m.

2.2 Simulation of Pavement Response to a Moving Load

Pavement response to moving loads was simulated for both rough and smooth surfaces [11]. Rough pavement surface, which excites the vehicle's suspension system, was modeled by using $\omega_0/2\pi = 1.23$ Hz and $\eta = 1$, while the smooth surface was modeled by

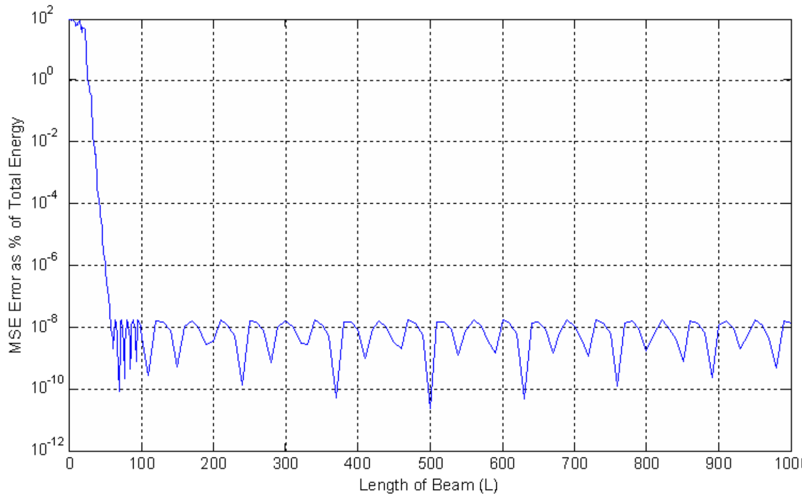

Figure 2.1: Relative mean square error in approximated solution

using $\eta = 0$. Figure 2.2, Figure 2.3, Figure 2.4, and Figure 2.5 show the results of the simulation [11]. Note that the signal arrives at any location x on the pavement before the truck arrives. In addition, the frequency of this signal decreases as the truck passes by the location. This is analogous to the Doppler effect, if we consider the vibrations as propagated waves and the pavement as the propagation medium.

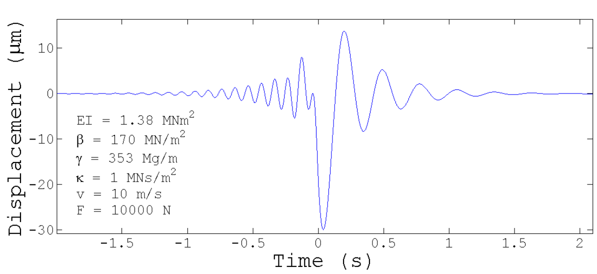

Figure 2.2: Displacement of rough surface

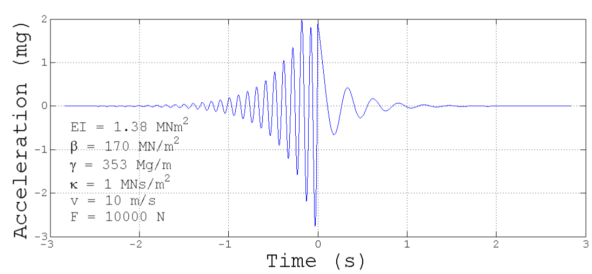

Figure 2.3: Acceleration of rough surface

Based on the simulated acceleration response of the pavement, Figure 2.3, we decided to build a sensor board which was able to resolve $\frac{1}{10}$th of this signal. In other

	ADXL203	MMA6233	SD1221-005
Range (± g)	1.7	10	5
Sensitivity (mV/g)	1000	120	800
P.S.D. RMS (μg/$\sqrt{Hz}$)	110	30	7
Power Consumption (mW)	3.5	7.26	40

Table 2.1: Comparison of Accelerometers

words, we aimed for a sensor board with a maximum noise of 200 μg RMS. In the frequency domain, the signal bandwidth appears to be less than 20 Hz but in order to account for any disparities between the theoretical model of the pavement and the actual pavement we decided to use a bandwidth of 50 Hz for our sensor board.

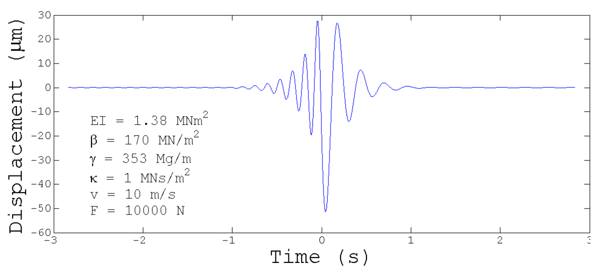

Figure 2.4: Displacement of smooth surface

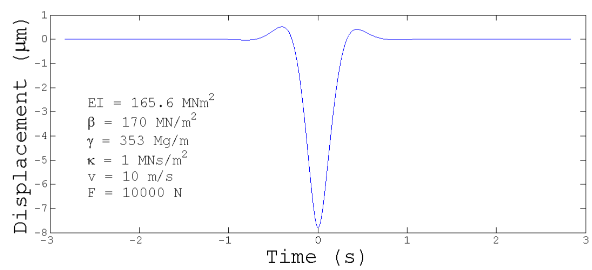

Figure 2.5: Displacement of smooth surface, EI = 166

2.3 Sensor Selection

We considered low noise accelerometers from three different vendors and Table 2.1 compares some of their important features [4, 2, 3].

The sensitivity (V/g) of an accelerometer is desired to be high because if the sensitivity is high even a small change in acceleration results in a large change in voltage and as a result can even be sampled by a low resolution analog-to-digital convertor. This reduces the cost of the sensor board and its power consumption. The power spectral density

(μg/$\sqrt{Hz}$), on the other hand, is a measure of how much noise is present in the output of the sensor at a given bandwidth. Thus, a lower power spectral density (PSD) is desirable. Since range and power consumption of the sensors were not the most important criteria in our case, the best sensor for the task was Silicon Designs 1221 (or SD1221-005) since it has the least PSD and also a reasonably high sensitivity. It is important to note that our sensor has the highest power consumption of all three. In some sense, we traded the power consumption for lower noise and higher sensitivity.[1]

2.4 Silicon Designs SD1221 Accelerometer

To test the performance of the selected accelerometer, we used the evaluation module [2] with additional circuitry on a prototyping board. Figure 2.6 describes the circuit used to test the accelerometer and Figure 2.7 is a photograph of the actual prototype board used. The power to the circuit was supplied through voltage regulators on the prototype board, which in turn were powered by batteries as shown in Figure 2.7.

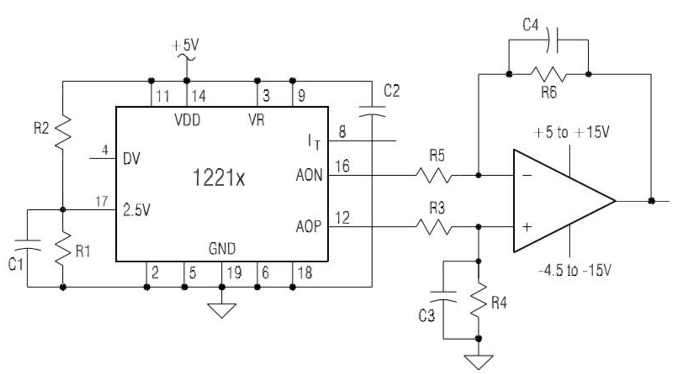

Figure 2.6: Prototype Circuit Schematic

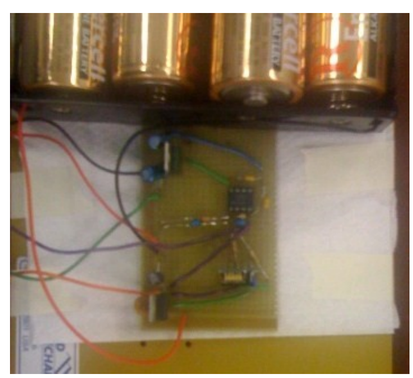

Figure 2.7: Prototype Circuit Board

[1] In actual measurements the power consumption was much lower $\approx$ 10 mW.
[2] Donated by Silicon Designs.

2.4.1 Circuit Description

The SD1221 chip is powered by a 5V source. The 2.5V reference, needed at pin 17, is created by using a voltage divider as shown. Capacitors C1 and C2 (0.1 μF each) are bypass capacitors to filter out the noise at the reference voltage pins, 3 and 17. Pin 8 (I_T), even though not used here, serves an important function. It can be used to sense the internal temperature of the chip. The nominal output current at 25°C is $\approx$ 500 μA and the nominal temperature sensitivity is 1.5 μA/°C [4]. This chip produces two analog outputs which vary with varying acceleration. At zero acceleration both these pins output a voltage of 2.5V but while AON decreases, AOP increases as acceleration increases. In other words, the difference between these two signals changes twice as much as individual outputs. To take advantage of this, we pass these signals through a difference amplifier/low-pass filter (cut-off 50 Hz), thus increasing the sensitivity and reducing the output noise. Note that increasing the sensitivity by amplifying the output signals reduces the range of the sensor. For instance, with an amplifier gain of 2.5, the range of a $\pm$ 5g sensor reduces to $\pm$ 2g due to clipping of the amplified signal at 5V by the amplifier.

2.4.2 Noise Measurement and Analysis

The power spectral density (ρ) of SD1221-005 accelerometer is typically 7 μg/$\sqrt{Hz}$. Thus, with a single pole low-pass filter($f_c = 50Hz$) the total power, due to a zero-mean gaussian noise, at the output can be calculated as [9]:

$$\begin{aligned}
\sigma^2 &= \int_0^\infty \frac{\rho^2}{1+(\frac{f}{f_c})^2} df \\
&= \rho^2 \frac{f_c \pi}{2}, \\
\Rightarrow \sigma &= \rho\sqrt{\frac{f_c \pi}{2}} \\
&= 62.04\ \mu g\ [for\ f_c = 50Hz,\ \rho = 7\mu g/\sqrt{Hz}].
\end{aligned}$$

Taking into account the sensitivity of the accelerometer and the amplifier gain (≈ 2.84), the theoretical RMS noise in the sensor should be approximately 141 μV.

Using a 24-bit ADC evaluation module from Analog Devices, we measured the final output voltage of the sensor board at a sampling rate of 1kHz. To convert the data acquired to acceleration, we had to calibrate the board for its sensitivity. We used precision gage blocks to change the inclination of the board, which was mounted on a calibration plate, and used the varying component of earth's gravity as applied acceleration. Since measured output was directly proportional to height of the gage blocks[3], we used linear regression to estimate the sensitivity of the device. It was found to be 1.973 V/g.

Figure 2.8 shows the results of our calibration. Every data point on this graph is actually the mean of 4096 samples collected for each inclination. The standard deviation and min/max in the figure show how much the individual samples varied from the mean.

Figure 2.9 shows the output of the sensor in the lab on a regular table and the output when the sensor is placed on a vibration proof optical table. An important observation is that the noise in the lab, and in any room equipped with computers or other electro-mechanical equipment, is of the same order as the expected transient vibrations on

[3]We develop the model for the calibration setup thoroughly in section 4.2.

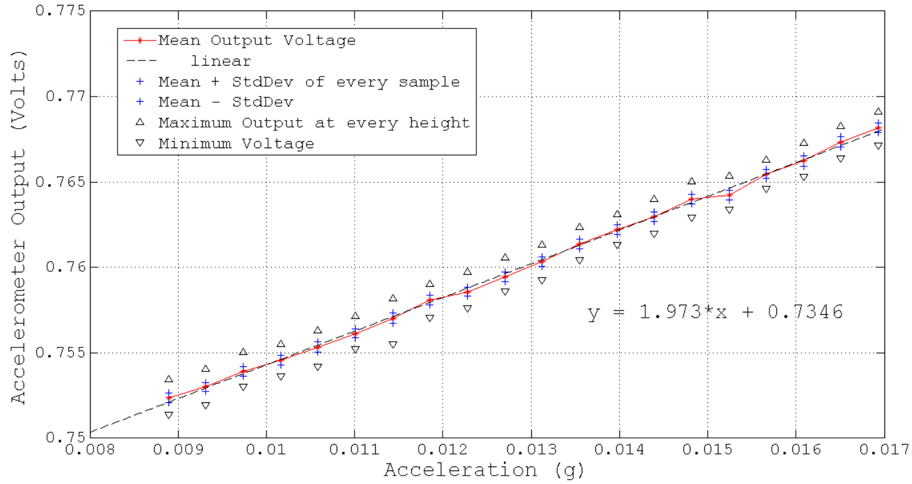

Figure 2.8: Calibration of the sensor board

the pavement due to a moving truck.

In addition, the device is very sensitive to any kind of sound in its vicinity as seen in Figure 2.10. The data in this figure was obtained by just clapping close ($\approx$ 2m) to the accelerometer. Note the peak in the frequency domain at around 400 Hz, even though this was attenuated ($\approx$ -18 dB) by the low-pass filter. This makes sense, however, because this peak lies in the audible range and is probably the frequency of the clapping sound. It was clear from this experiment that sound had to be isolated from the sensor, in order for the sensor output to be meaningful when installed on the pavement. We discuss a solution for this problem in chapter 4 and chapter 5.

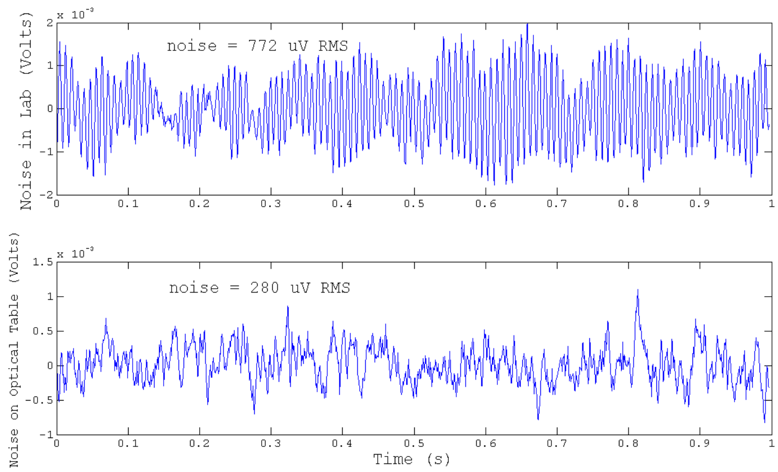

Figure 2.9: Noise from the accelerometer board

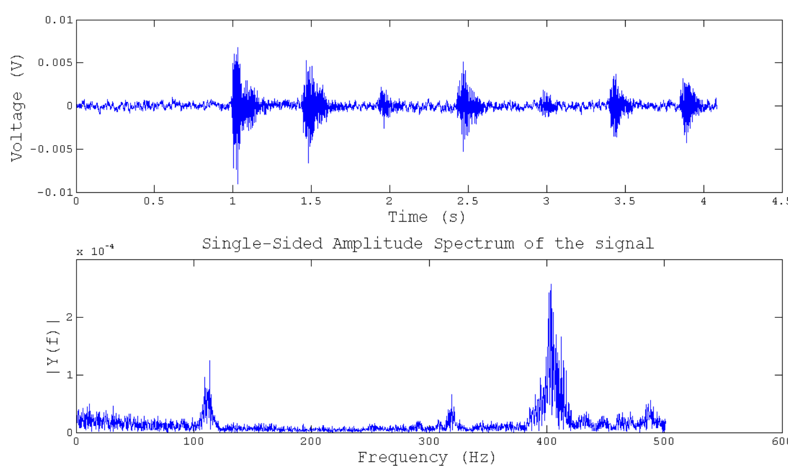

Figure 2.10: Accelerometer response to sound

Chapter 3

Sensor Board and Packaging

In this chapter we discuss the circuit design of the sensor board and its printed circuit board (PCB) layout. We then discuss the packaging of the sensor board and the installation procedure chosen to minimize the effect of external noise on the sensor.

3.1 Sensor Board

A key luxury present while prototyping was the availability of dual power supplies. Unfortunately, it is rarely the case that an embedded sensor uses two batteries and the negative rail of the amplifier is usually grounded. This is done to save energy or to save space occupied by the system. Another difference is that in order to measure the vibrations perpendicular to the plane of the pavement, we must place the sensor such that its sensing direction is aligned with the acceleration due to gravity (g). This means that the sensor will have a DC offset corresponding to the measurement of g. These two differences pose problems but both have a common solution. By carefully adjusting the gain of the amplifier, we can make sure that this DC offset lies between 2V and 3V (roughly midway between 0 and 5V). Thus, any small amplitude vibrations would result into a small amplitude output signal centered at this DC offset i.e. a small signal superimposed on a large DC signal.

3.1.1 Circuit Schematic

Figure 3.1 shows the circuit schematic of the sensor board. The circuit is quite similar to the prototype circuit shown in Figure 2.6, except for a few new components.

Only one battery is used to power the entire board and it is a rechargeable 3.6V NiMH battery. The main switch (SW1) connects/disconnects the battery to the voltage regulator. LTC1682-5 is a low noise (60 μV_{RMS} at 100 kHz BW), low power consuming (150 μA) double charge pump voltage regulator, which converts 3.6V to 5V [6]. AD8542 amplifiers are also very low power consuming (45 μA/amplifier) and low noise (noise density $\approx$ 40 nV/$\sqrt{Hz}$) [5]. Two screw clamps, shown as OutPins in the schematic, are used to connect the data-acquisition box to different test points on the board. Note that pin 8 (I_T), unlike the prototype board, is connected to a 2 kΩ resistor so that internal temperature of the chip can be sensed by just measuring the voltage across that resistor.

3.1.2 PCB Layout

Figure 3.2 shows the layout of the sensor board.[1] The layout gerber files, along with the parts ordered from Digi-Key Corp., were sent for PCB manufacturing and assembly. Figure 3.3 shows the resulting sensor board.

[1]Both the schematic and the PCB layout were completed using the freeware version of EAGLE Layout Editor.

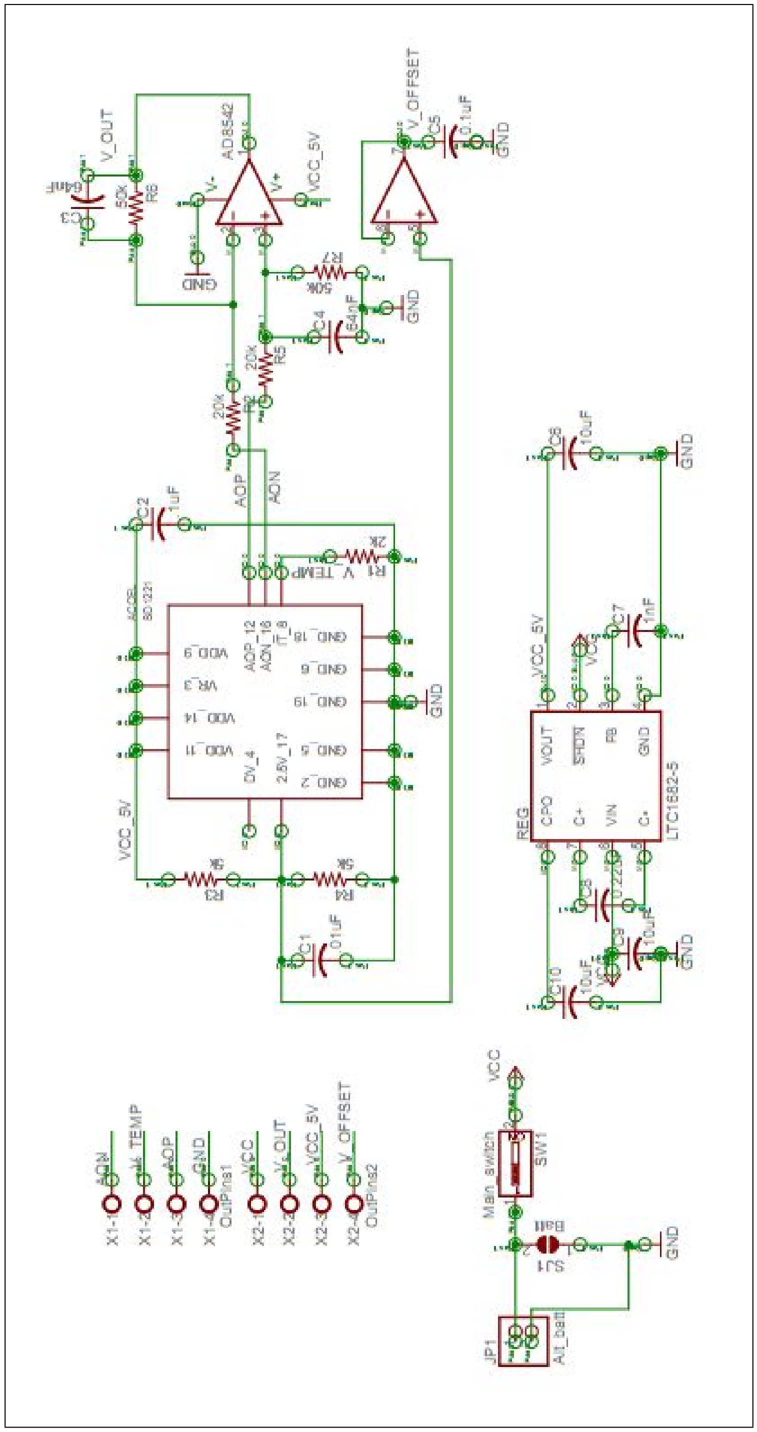

Figure 3.1: Circuit schematic

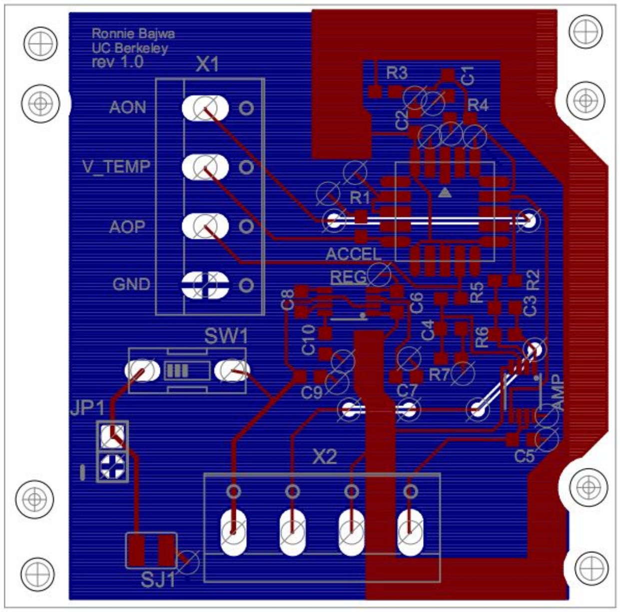

Figure 3.2: PCB layout of the sensor board

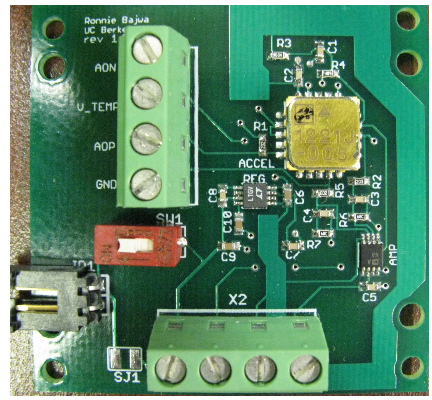

Figure 3.3: Picture of the sensor board

3.2 Packaging and Installation of Sensor Board

As discussed before, the sensor board must be isolated from external noise. The sensor must also have a good coupling with the pavement to measure the signal accurately. Further, if the sensor has to be embedded in a pavement its packaging must be strong enough to withstand the pressure exerted on it by vehicles moving on the road. Finally, to increase the lifetime of the sensor board it must be protected from water, air and other chemicals. To achieve all of these goals, we used the packaging designed by Sensys Networks for their vehicle detection system.

3.2.1 Sensor Package

Figure 3.4 shows the small, hard plastic case used. To prevent the sensor board from water, air etc. the case was filled with fused silica. Since our sensor board was not

Figure 3.4: Sensor case, courtesy of Sensys Networks

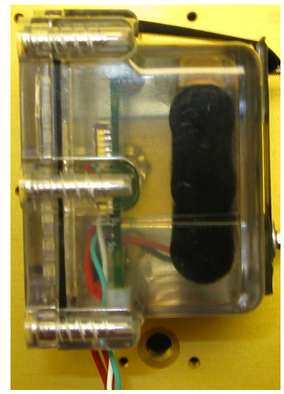

Figure 3.5: Potted sensor

capable of wireless communication yet, we drilled a small hole on the side of this casing to let the relevant wires out as shown in Figure 3.5.[2]

3.2.2 Sensor Installation Procedure

Figure 3.6: Sensor installed on concrete pavement

Installation of each sensor takes less than 10 minutes. Installation simply requires boring a 4-inch / 10-cm diameter hole approximately 2 $\frac{1}{4}$ inches / 5.7 cm deep at the

[2]Thanks to Sensys Networks for getting the sensor potted.

desired location, placing the sensor into the hole so that it is properly leveled with the earth's surface, and sealing the hole with fast-drying epoxy [1]. To bury the wires in the pavement, we made a saw cut to the side of the pavement and filled it with fast-drying epoxy. Figure 3.6 shows the sensor installed in a concrete pavement.

Chapter 4

Sensor Calibration and Noise Analysis

In this chapter we discuss how we calibrated the sensor for its sensitivity (V/g), offset, resolution, and the frequency response. After calibrating the sensor, we tested how sound affected the sensor and how to minimize its effect.

4.1 Calibration Model

Figure 4.1 models the calibration setup used and Figure 4.2 is a picture of the actual setup. The idea is to use gage blocks of different heights to change the inclination of the sensor box, thus changing the component of acceleration due to gravity (g) along the sensing direction of the accelerometer. Using simple geometry, the component along the sensing axis of the accelerometer is $g\cos(\theta_1 + \theta_2 - \theta_3)$. Thus, the output voltage (v) must be:

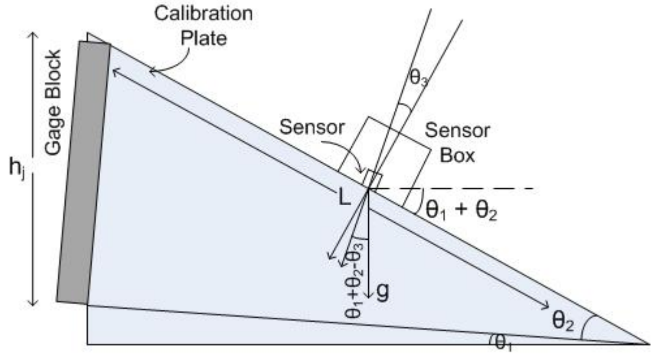

Figure 4.1: Calibration Setup

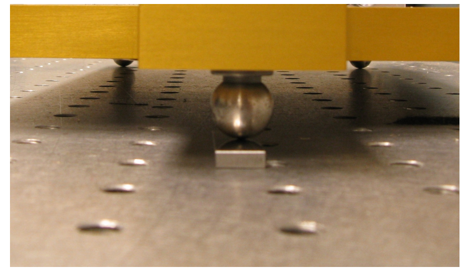

Figure 4.2: Picture of the calibration plate/gage block

$$
\begin{aligned}
v &= \alpha g \cos(\theta_2 - \theta) \\
&= \alpha g \cos\theta_2 \cos\theta + \alpha g \sin\theta_2 \sin\theta \\
&= \mathrm{A}\cos\theta_2 + \mathrm{B}\sin\theta_2 \\
&= \mathrm{A}\sqrt{1-\left(\frac{h}{L}\right)^2} + \mathrm{B}\left(\frac{h}{L}\right) \\
&= \mathrm{A}\sqrt{1-x^2} + \mathrm{B}x. \qquad (4.1) \\
\alpha &= \sqrt{\mathrm{A}^2 + \mathrm{B}^2}. \qquad (4.2)
\end{aligned}
$$

v : output voltage

α : Sensitivity in V/g

θ : net tilt, $\theta_3 - \theta_1$

h : height of gage block

L : length of calibration plate

$\mathrm{A} = \alpha g \cos\theta$, $\mathrm{B} = \alpha g \sin\theta$

$x = \frac{h}{L}$

In reality, the measured output is never constant and fluctuates around some mean value due to noise in the surroundings and electronics. We model this by adding a zero mean gaussian random variable to equation (4.1). In addition, we noticed that every time the device was turned on even the average output value was slightly different. Thus, another random variable with a non-zero mean was added to model this offset. Note that this offset changes only when the sensor is turned off and then turned back on, it remains constant during sampling of the output signal. Equation (4.3) incorporates these additions to the model.

$$v_{i,j} = \mathrm{A}\sqrt{1 - x^2} + \mathrm{B}x + \mathrm{C}_j + \xi_{i,j}. \tag{4.3}$$

A Trial : sensor is turned on, output sampled, sensor turned off

j : trial number

i : sample number of data collected during a trial

$\xi_{i,j}$: zero mean gaussian random variable

C_j : random variable modeling offset

4.2 Calibration Procedure and Results

The model developed above was used in sections below to estimate the useful properties of our sensor. It is worthwhile mentioning one key difference between the crude calibration procedure discussed in section 2.4.2 and the procedure followed here. In case of the prototype board, the sensor orientation was perpendicular to the earth's gravity and thus it measured $g \sin(\theta_2 - \theta)$, refer to Figure 4.1. However, the calibration setup used for calibrating the sensor board measured $g \cos(\theta_2 - \theta)$ and this is more relevant since the sensor will be installed on the pavement in the same orientation.

4.2.1 Sensitivity Calibration

To estimate A, B and thus the sensitivity (α), given by equation (4.2), we measured the sensor output at different inclinations.[1] At every inclination we collected 2000 samples (sampling frequency: 2 kHz, for total time of 1s) of data. We averaged the output over

[1] All voltage signals were measured by National Instruments 24-bit data acquisition box.

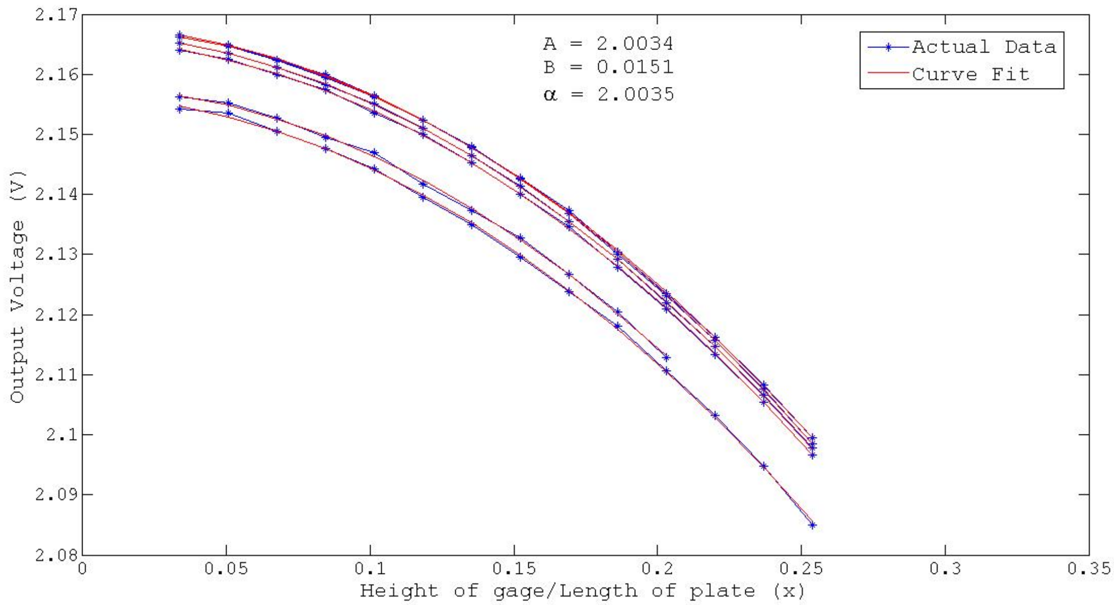

Figure 4.3: Results of sensitivity calibration

these samples at every inclination and assumed that the average noise is approximately zero. This is a valid assumption since the average noise approaches its true mean, zero, as the number of samples increase [7]. We then used linear regression to estimate the A, B, and C_j in equation (4.4).

$$\bar{v}_j = A\sqrt{1 - x^2} \; + \; Bx \; + \; C_j. \tag{4.4}$$

To improve the accuracy of results, we repeated the sensitivity calibration six times and used the average estimate of A, B to calculate α. Figure 4.3 shows the results. Note how the offset C_j is different in all cases, thus justifying the use of j in equation (4.4).

4.2.2 Sensor Noise and Resolution

In our model and in the regression analysis, we assumed that $\xi_{i,j}$ were independent and identically distributed random variables. If this were the case, data from such a distribution should be uncorrelated [7]. However, in our case the noise is passed through a low pass filter, so some degree of correlation is expected in the data. Figure 4.4 and its zoomed version, Figure 4.5, compare the auto-correlation of sensor data and software generated and filtered white noise. Since there is great agreement in the two, it is safe to assume that the noise from the sensor is independent and identically distributed.

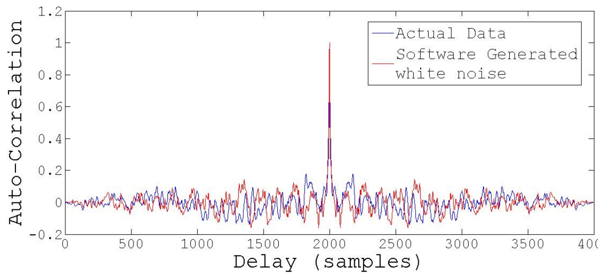

Figure 4.4: Auto-correlation of sensor noise

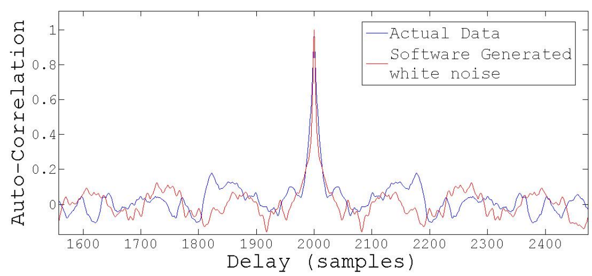

Figure 4.5: Zoomed in version of Figure 4.4

To calculate the noise, or the estimate of standard deviation of $\xi_{i,j}$ in case of our model, we use the data collected in all the trials of sensitivity experiment. The RMS noise was calculated to be about 383 μV or 191μg. This number gives us a measure of the resolution of our sensor board.

4.2.3 Calibration for Sensor Offset

To estimate the mean offset, we turn the sensor on/off a number of times (M) and sample the sensor output each time, collecting N samples. We keep the inclination the same, and in reference to our model (equation (4.3)) we chose x=0. The unbiased estimator

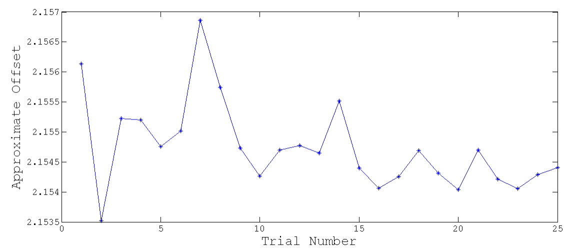

Figure 4.6: Offset Variation

for the expected value of the sensor offset is given by:

$$\hat{\mu_C} = \frac{1}{MN}\sum_{j=0}^{M}\sum_{i=0}^{N} V_{i,j} - \hat{A}. \tag{4.5}$$

$\hat{A}$ is the estimate of A. Figure 4.6 shows the offset from M=25 trials of sensor turn on/off. The estimated expected value of offset from this data was 0.1513 V and the estimated standard deviation of offset was 1.63 mV. We can find an expression for the mean square error of μ_C as

$$v_{i,j} = A + C_j + \xi_{i,j}. \tag{4.6}$$

If $\hat{A}$ is an unbiased estimator, so is $\hat{\mu_C}$ i.e.

$$E[(\mu_C - \hat{\mu_C})^2] = \sigma^2(\mu_C).$$

Thus, using equation 4.5 and equation 4.6

$$\sigma^2(\mu_C) = \frac{\sigma_{i,j}^2}{\text{MN}} + \frac{\sigma_C^2}{M} + \sigma_A^2. \tag{4.7}$$

Thus, we can increase the accuracy of $\hat{\mu_C}$ by increasing the number of samples collected in every trial or by increasing the number of trials but it can only be as accurate as our estimate of A.

4.2.4 Frequency Response

It is important to know whether the sensor responds differently to excitations of different frequencies. Thus, the need to find the frequency response of the sensor. The accelerometer board was mounted on a shaker table at Richmond Field Station (RFS) and the output of the sensor was compared to their reference accelerometer (Setra 141a). Figure 4.7 and Figure 4.8 show the setup.

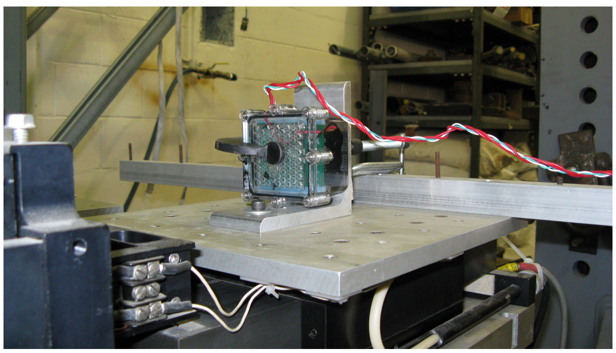

Figure 4.7: Shaker Setup [Front view]

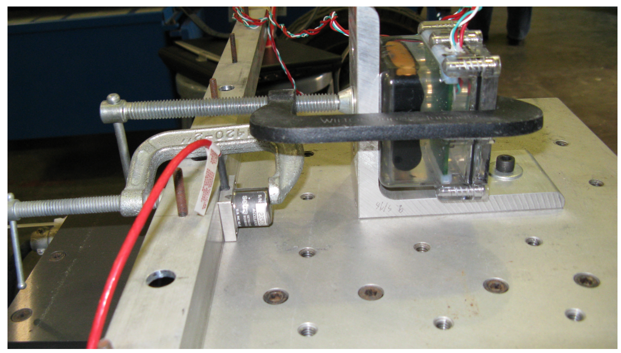

Figure 4.8: Shaker Setup [Side view]

The data acquisition system at RFS had a built in 4th order low-pass Bessel filter for anti-aliasing and collected the data at a sampling frequency of 500 Hz. In addition to this filter, our accelerometer had a one-pole (at 50 Hz) low-pass filter while the reference accelerometer did not have this additional filter. Thus, in order to compare the sensor output with the reference accelerometer output, the sensor data was scaled to undo the attenuation due to this filter. Figure 4.9 and Figure 4.10 show the measured output, both in time and frequency domain, when the shaker table was driven at 4Hz.

Figure 4.11 and Table 4.1 show the comparison of the gain, ratio of output signal (RMS) to the input signal(RMS), of the sensor board and the reference accelerometer.[2]

[2] The DC offset in the two outputs was also subtracted for meaningful comparison.

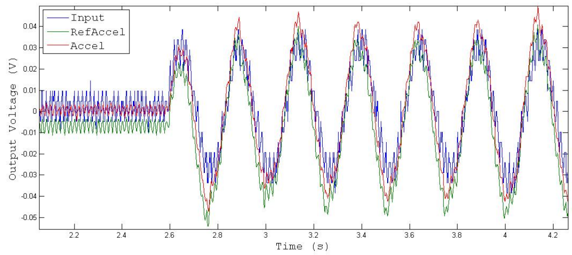

Figure 4.9: Output at 4Hz excitation

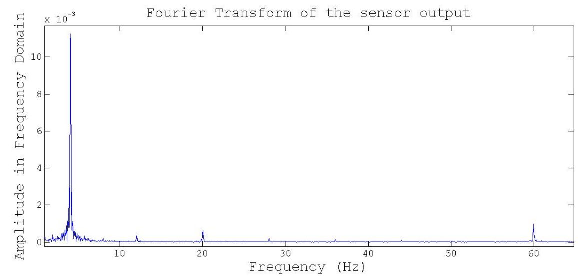

Figure 4.10: Fourier Transform of the output

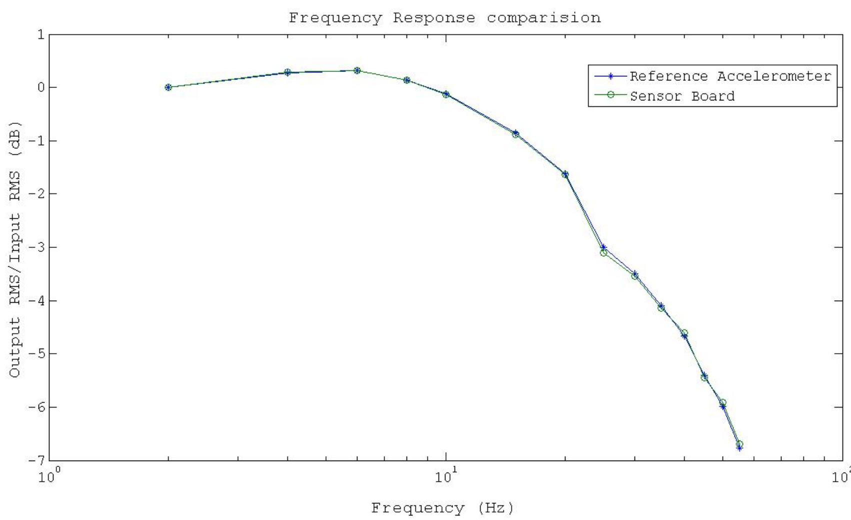

Figure 4.11: Comparison of frequency response

The RMS discrepancy was calculated to be .05 dB. Clearly, the frequency response of the sensor board is almost identical to that of the reference accelerometer.

4.2.5 Calibration results

Table 4.2 summarizes the results from the calibration.

Frequency (Hz)	Accel RMS Gain (dB)	Ref. Accel RMS Gain (dB)	Discrepancy (dB)
4	0.2804	0.2744	0.006
6	0.3231	0.3223	0.0008
8	0.1371	0.1337	0.0034
10	-0.1259	-0.1242	-0.0017
15	-0.8774	-0.8472	-0.0302
20	-1.6376	-1.6122	-0.0254
25	-3.1018	-2.9974	-0.1044
30	-3.5347	-3.5026	-0.0321
35	-4.148	-4.1031	-0.0449
40	-4.6053	-4.6634	0.0581
45	-5.4538	-5.4043	-0.0495
50	-5.9136	-5.9875	0.0739
55	-6.6849	-6.762	0.0771

Table 4.1: Comparison of frequency response

A ($\alpha g \cos(\theta)$)	B ($\alpha g \sin(\theta)$)	Sensitivity (V/g)	RMS Noise (V)	Mean Offset (V)
2.0034	0.0151	2.0035	191	0.1513

Table 4.2: Calibration results

Figure 4.12: Setup for sound experiment

4.3 Isolation of the sensor from sound

To test the sensor for sound sensitivity we played loud monotones, generated using MATLAB, and analyzed the sensor output for noise. Figure 4.12 shows the setup used. To emulate field conditions, where the sensor will be buried in the pavement, we placed the sensor in two concrete disks and sealed all the gaps.

Sound was played using two $10W$ speakers at full volume but the exact decibel level was not measured. Figure 4.13 shows the output signal of the sensor when no sound was played. The RMS noise measured was 163 μg, which is actually less than what we found in section 4.2.2. This is probably because the setup is sealed from any air gaps in this case. The frequency spectrum looks as expected. There is attenuation of higher frequencies of the wide-band noise due to the low pass filter.

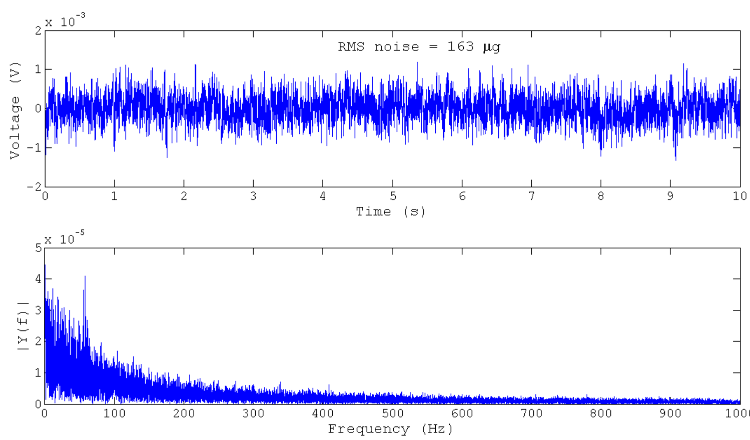

Figure 4.13: Sensor output without sound

Figure 4.14 shows the output when a monotone at 20Hz was played. The RMS noise increased to 564 μg. However, if we look at the frequency spectrum of the signal we realize that a lot of the noise is at frequencies higher than 50 Hz. This is peculiar not only because the sound played was a 20 Hz monotone, but also because even after the attenuation by the 50 Hz filter the higher frequency noise is dominant. It is very likely that since most of the higher frequency noise is at higher harmonics of 20 Hz, the speaker behaved in a non-linear fashion and generated sound at higher harmonics. However, it is likely that the problem can be dealt by using a higher order low-pass filter.

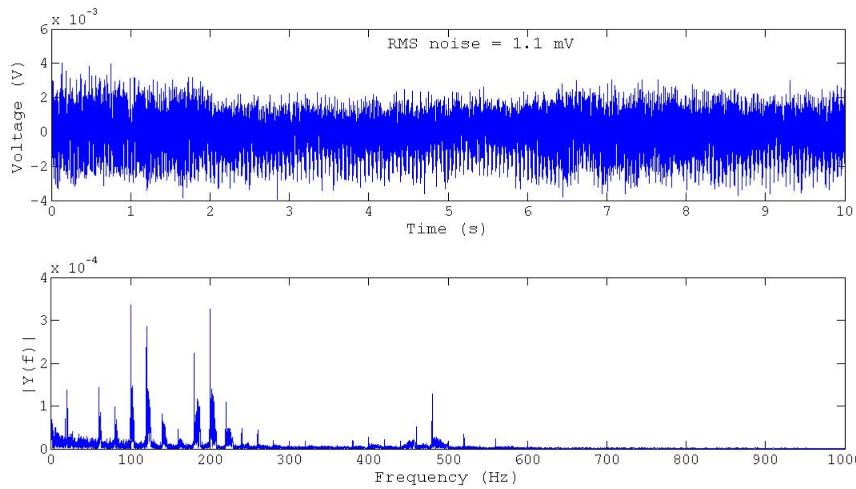

Figure 4.14: Output with 20Hz monotone

Figure 4.15 shows the same output as in Figure 4.14, but after filtering the signal digitally using a 4th order low-pass butterworth filter. The RMS noise decreased to 170 μg.

Table 4.3 compares the noise of the digitally unfiltered and filtered data when monotones at different frequencies were played. It is important to notice that noise in the filtered case was less than 200 μg in most cases. Thus, theoretically the sensor can be made immune to sound such that it responds only to pavement vibrations since any noise less than the aimed resolution of 200 μg is acceptable.

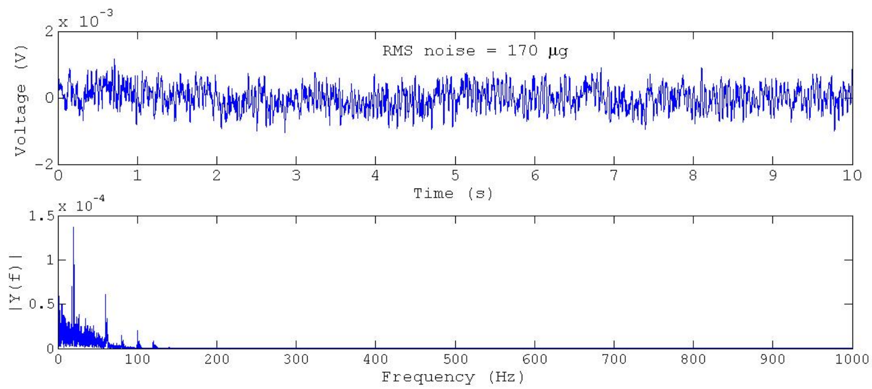

Figure 4.15: Filtered output with 20Hz monotone

Frequency of Tone (Hz)	Unfiltered Noise (μg RMS)	Filtered Noise (μg RMS)
no sound	163.18	119.91
20	564.46	170.30
30	933.52	175.34
40	2603.39	206.64
50	768.75	170.19
500	3046.52	155.63

Table 4.3: Comparison of noise before and after digital filtering

4.3.1 Anti-Aliasing Filter Design

Although filtering in software reduced the noise to the desired level, this might not be the best approach. Currently, we were sampling at 2 kHz and using a data acquisition box. But in future, we will have a micro-controller on board and would like to sample at a much smaller rate to save energy. In that case, aliasing could lead to a lot of low frequency noise. To avoid this and to reduce the noise due to sound as well, we can use a better anti-aliasing filter on the sensor board. For testing purposes, we connected the output of the sensor board to a 3rd order low pass filter such that signal from the accelerometer passes through a net 4th order low pass filter before getting sampled. Table 4.4 compares the noise after filtering the output by a 1st order and a 4th order low pass filter.

Frequency of Tone (Hz)	Filtered Noise (1-pole) (μg RMS)	Filtered Noise (4-pole) (μg RMS)
no sound	214.4	158.6
20	613.3	182.8
30	986.3	229.8
40	1100	206.1
50	311.2	199.3
500	274.6	154.8

Table 4.4: Comparison of noise with different filters

Once again, the noise decreases to the desirable level in most cases with the use of a 4-pole low pass anti-aliasing filter.

Chapter 5

Sensor Testing on Concrete Pavement

The calibrated sensor was installed in a concrete pavement using the installation procedure described in section 3.2.2. In this chapter, we discuss the various experiments done to test the sensor board.

5.1 Falling Weight Deflectometer Tests

A falling weight deflectometer (FWD) is a commonly used testing device to evaluate the properties of the pavement. It consists essentially of a large mass that is constrained to fall vertically under gravity on to a spring-loaded plate resting on the pavement surface. The mass itself is cylindrical in shape and is dropped from different heights to apply different loads. A load cell mounted on top of the load plate measures the load imparted to the pavement surface. Deflection sensors, usually geophones, attached in line with the center of the load plate are used to measure deflections at various points, which can then be used to determine the physical properties of the pavement [13]. The main advantage of using a FWD to test our sensor is that it simulates the actual loads produced by moving vehicles and we can compare our sensor output with the data collected by the deflection sensors.

5.1.1 Experimental Setup

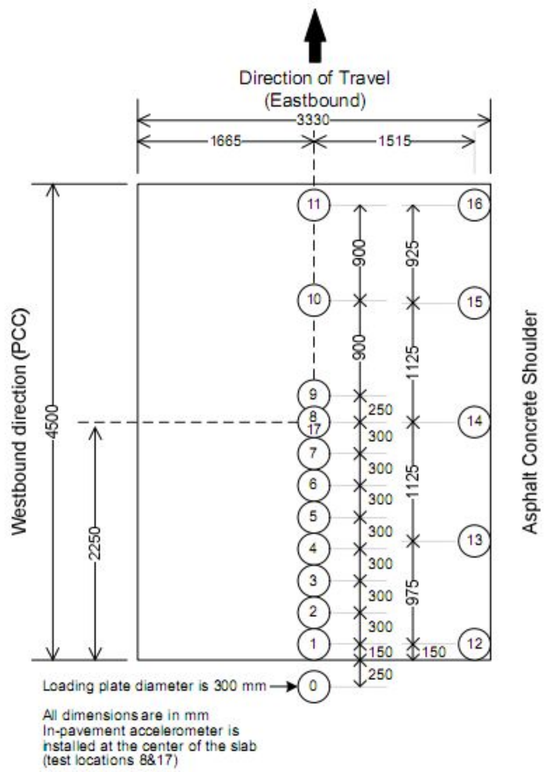

Figure 5.1: FWD load locations

Figure 5.1 shows the different places FWD load was applied. The sensor board was installed at the center of the concrete slab, location 8, and there were eight different deflection sensors that measured deflection of the pavement at multiple locations.

5.1.2 Comparison of sensors

Figure 5.2 shows one example of signal measured by our sensor when a load of 9000 lb was applied at location 9.

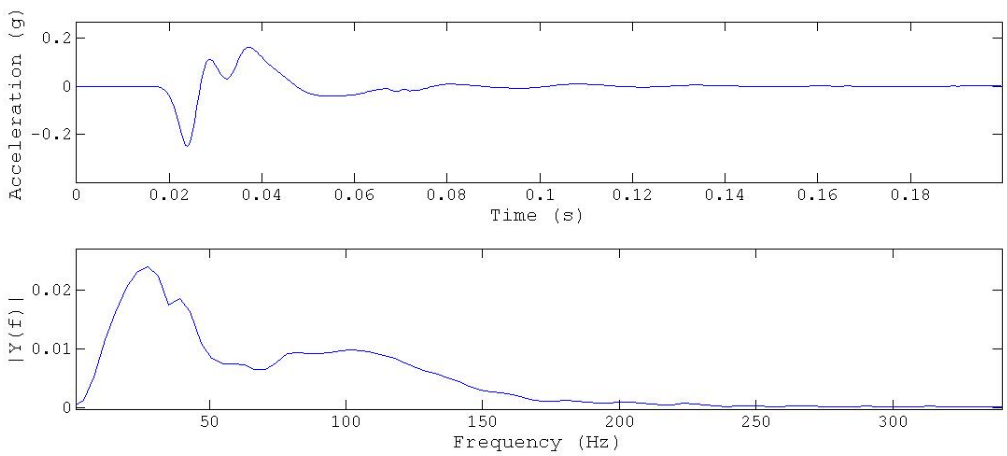

Figure 5.2: Acceleration due to 9000 lb load

To test the accuracy of our sensor board, we compared the data collected by our sensor with the data collected by the closest deflection sensor. In one instance, when a load[1] was applied at location 9, the closest deflection sensor was at the same location as the sensor board.[2] Figure 5.3 shows that both the signals measured are in close agreement.[3]

5.1.3 Impulse Response of the Pavement

Since the pavement is isotropic and very long, measuring the signal at location 8 after applying a load at location x is the equivalent to measuring the signal at location x

[1]In Figure 5.3, output was normalized to represent an applied load of 50,000 N.

[2]There could be an error of ± 0.5 cm due to the inaccuracy in loading plate placement.

[3]To obtain the displacement from acceleration, we used double integration and adjusted for the drift due to white noise integration.

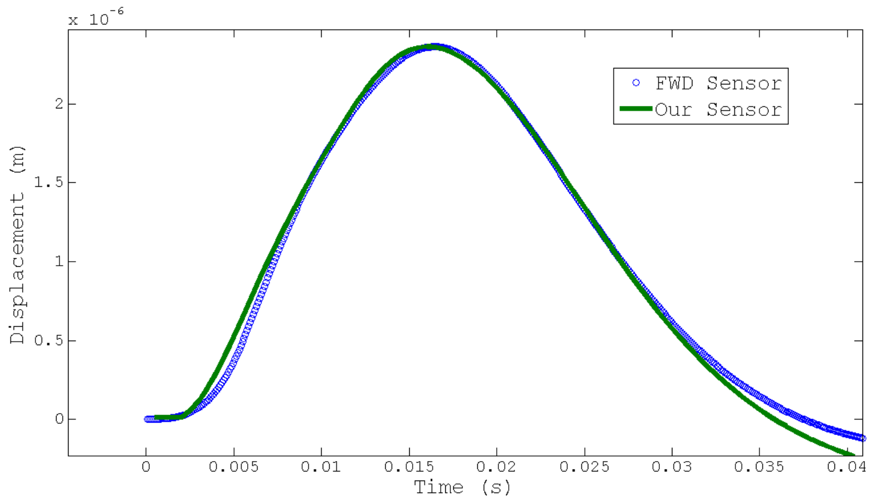

Figure 5.3: Comparison of the measured displacements

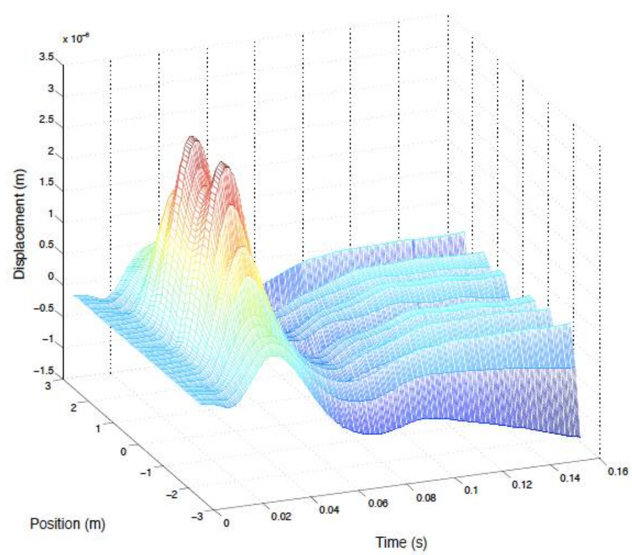

Figure 5.4: Impulse response of the pavement

after applying the load at location 8. Thus, we can think of our experiment as if the load was applied at location 8 and signal was measured at different locations by using multiple sensors. We use this fact and the data collected from our sensor board to calculate the impulse response of the pavement, shown in Figure 5.4.

5.2 Experiments Using a Real Truck

Figure 5.5: Picture of the truck used

We drove the truck, shown in Figure 5.5, on the pavement at different speeds and measured the transient vibrations using our installed sensor board. In addition, we stopped the truck over the sensor and tested the sensor against the different types of sounds/vibrations produced by the vehicle.

5.2.1 Vibrations Due to a Moving Truck

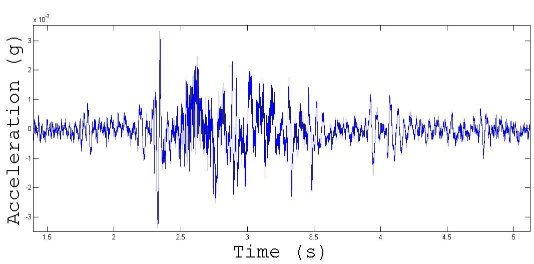

Figure 5.6: Truck at 15 mi/hr

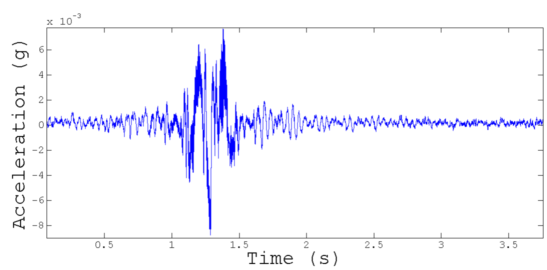

Figure 5.7: Truck at 55 mi/hr

Figure 5.6 and Figure 5.7 show the vibrations due to the truck moving at 15

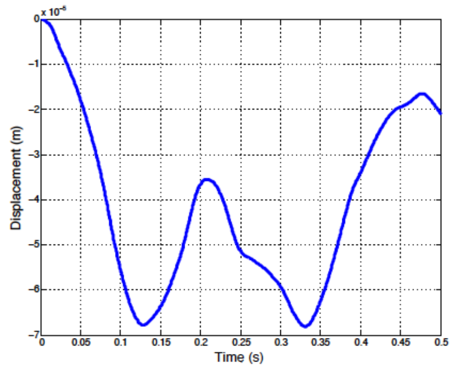

Figure 5.8: Double integration of displacement

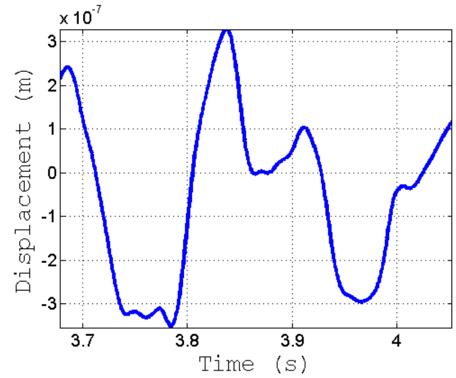

Figure 5.9: Double integration with forgetting factor

mi/hr and 55 mi/hr respectively. The signal to noise ratio (SNR) is not as high as the FWD experiment but nevertheless it is enough to detect the passage of the truck. It is important to note that commercial trucks are much heavier than the truck used in this experiment. While the front axle weighed approximately 7000 lb for this truck, it can be as high as 20,000 lb for a commercial truck. We plan to collect more data using commercial trucks in order to develop an algorithm which can successfully calculate weight of the vehicle from the vibrations measured.

Figure 5.8 shows the displacement calculated by double integration of acceleration. Each axle applies a dynamic load to the pavement and thus causes a displacement trough. In case of this truck, however, the second and the third axle were very close to each other and thus it is very hard to distinguish them in this image. Figure 5.9 shows the double integration of acceleration but with the use of a forgetting factor to reduce the effect of the past samples on the current value being calculated through integration. The idea is to reduce the effect of adjacent axle loads and give more importance to the current axle load. The three main troughs in Figure 5.9 seem to capture this idea and appear to represent the axles of this truck.

5.2.2 Sound Isolation of the Sensor

As previously discussed, if sound is not isolated from the sensor board the signal to noise ratio of the sensor deteriorates. To check that we effectively isolated sound from the sensor, we stopped the truck over the sensor and measured the output of the sensor when the engine is off, when the engine is just started but not revved, when the engine is revved up, and when the truck's horn is blown. Table 5.1 summarizes the noise in these cases.

	RMS Noise (ug)
engine off	160
engine on but not revved	171
engine revved	231
engine off but horn blown	167

Table 5.1: Effect of truck noise

Note that when the engine is revved up, the noise increase to 231 μg but this is an exaggeration of any real situation. Even in this case though, the noise is close to 200 μg. Since the targeted noise was 200 μg RMS, we have successfully isolated our sensor from sound.

Chapter 6

Conclusion

6.1 Accomplishments

A highly sensitive, low noise sensor board using MEMS accelerometer technology was designed, fabricated and tested. The board is capable of resolving accelerations as low as 200 μg. The sensor board was successfully isolated from sound by a combined use of packaging, installation procedure, and low-pass filtering. The sensor board was installed in a concrete pavement and compared well with the deflection sensors of a falling weight deflectometer when the pavement was excited. The sensor was able to measure the vibrations due to light truck moving on the pavement at different speeds and appears to successfully detect individual axles of the vehicle.

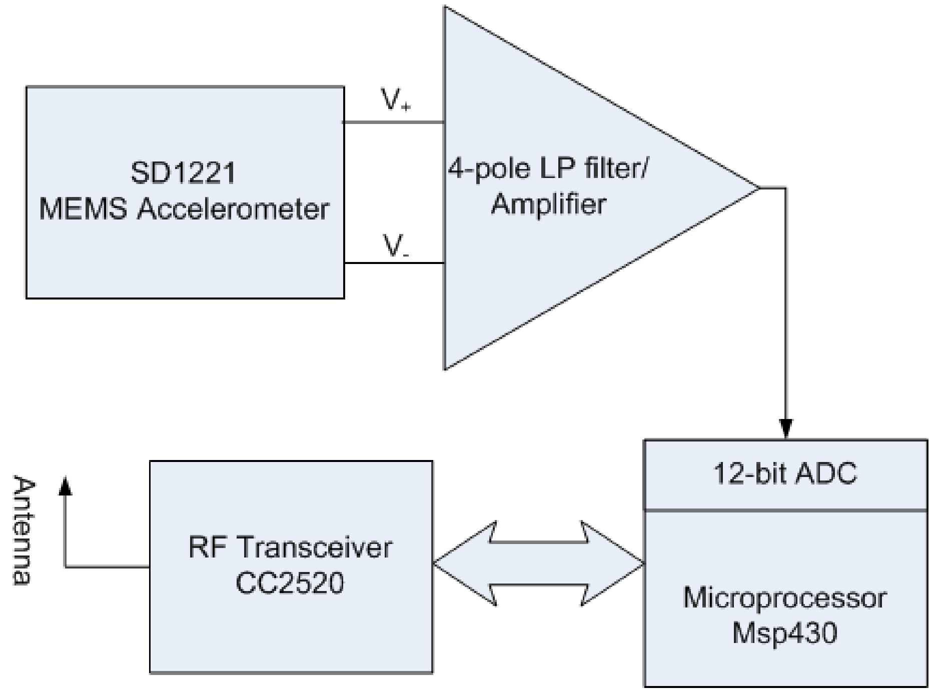

Figure 6.1: Block diagram of the system

6.2 Future Work

In thee plan on driving commercial trucks with different weights on the pavement and using the data to verify and extend the model developed in [12]. This data will also be used to design and test the algorithm that can calculate the load of a moving vehicle from the measured acceleration. We realize that it would be helpful to have multiple sensors on the pavement instead of just one but the wired version of the sensor is not ideal for this purpose. Thus, we will be designing a wireless version of this sensor. Figure 6.1 shows the block diagram of the entire system.

We have already tested the accelerometer/filter combination of this diagram. We are almost finished with the addition of the micro-controller on the circuit board but more work needs to be done to add a radio on-board.

Applications

Even though the system described here is aimed at building a WIM system, it can be used in a variety of other applications:

Axle Counting: The number of axels in a truck can be detected from the acceleration measurement by converting it to displacement, as discussed in section 5.2.1. This is an important application and currently there are a very limited number sensors for this purpose.

Pavement Damage Meter: The acceleration measurement can be converted to an estimate of how much the pavement is being damaged as well. Some existing methods associate the average observed weights to damage [8], but direct response analysis could potentially be used.

FWD Replacement: Falling Weight Deflectometers are currently used to test pavement response. A FWD drops a known weight on the pavement and measures the pavement response. The cost of transporting the equipment to the test location and its calibration can be quite high. Instead, embedded sensors in the pavement could record pavement response to trucks that regularly use those roads. The pavement response can be inferred from this measurement. One major advantage of using embedded sensors is that one can measure the pavement response at different depths by installing the sensor at the desired depths, whereas this is not possible with a FWD.

Structural Monitoring: Embedding our sensor in various structures such as beams in buildings, bridges, etc. allows for permanent monitoring of structural integrity.

Seismic Monitoring: The very high resolution of our sensor makes it capable of measuring even the lowest level seismic activity and thus can be used to collect seismic data over the air (once we add radio to the board).

Airport Runway Monitoring: Our sensor could also be used to monitor and test the airport runway pavement.

Bibliography

[1] The Sensys$^{\mathrm{tm}}$ wireless vehicle detection system: Advanced technology for 21st century traffic management. http://www.sensysnetworks.com/userfiles/whitepapers/sensys_system_overview_v1.10.pdf. [cited at p. 18]

[2] Precision ±1.7 g single/dual axis accelerometer. http://pdf1.alldatasheet.com/datasheet-pdf/view/83692/AD/ADXL203.html, 2004. Rev. 0. [cited at p. 7]

[3] ±10 g dual axis micromachined accelerometer. http://www.freescale.com/files/sensors/doc/data_sheet/MMA6231Q.pdf, October 2006. Rev. 2. [cited at p. 7]

[4] Model 1221 low noise analog accelerometer. http://www.silicondesigns.com/pdfs/1221.pdf, Sept. 2007. [cited at p. 7, 9]

[5] General-purpose cmos rail-to-rail amplifiers ad8541/ad8542/ad8544. http://www.analog.com/static/imported-files/data_sheets/AD8541_8542_8544.pdf, January 2008. Rev. F. [cited at p. 14]

[6] Ltc1682/ltc1682-3.3/ltc1682-5 doubler charge pumps with low noise linear regulator. http://cds.linear.com/docs/Datasheet/168235fs.pdf, January 2008. Rev. F. [cited at p. 14]

[7] Dimitri P. Bertsekas and John N. Tsitsiklis. *Introduction to probablility*. Athena Scientific, 2002., third edition. [cited at p. 22, 23]

[8] David Cebon. Vehicle-generated road damage: A review. *Vehicle System Dynamics: International Journal of Vehicle Mechanics and Mobility*, 18:107–150, 1989. [cited at p. 41]

[9] John A. Gubner. *Probability and random processes for electrical and computer engineers*. Cambridge ; Cambridge University Press, 2006. [cited at p. 9]

[10] Lianhe Guo, Yumei Tang, Jingyan Yu, Jing Li, Xuemin Chen, and Richard Liu. Weigh-in-motion system design with piezoelectric sensor. volume 153. ASCE, 2004. [cited at p. 1]

[11] Ram Rajagopal. Large monitoring systems: Data analysis, design and deployment. PhD dissertation at UC Berkeley, forthcoming, 2009. [cited at p. 5, 6]

[12] Ram Rajagopal, Alexander B. Kurzhansky, and Pravin Varaiya. A low-cost wireless mems system for measuring dynamic pavement loads. Technical Report UCB-ITS-PRR-2008-36, California Partners of Advanced Transit and Highways, 2008. [cited at p. 1, 3, 4, 5, 40]

[13] Boutros Sebaaly, Trevor G. Davis, and Michael S. Mamlouk. Dynamics of falling weight deflectometer. *Journal of Transportation Engineering*, 111(6):618–632, 1985. [cited at p. 33]

[14] George Yannis and Constantinos Antoniou. Effect of weigh-in-motion system measurement errors on load-pavement impact estimation. *Journal of Transportation Engineering*, 133, 2007. [cited at p. 2]